Electrical properties and reactivity under air-CO flows of composite systems based on ceria coated carbon nanotubes

Marjorie David, Madjid Arab, Frédéric Guinneton, Emmanuel Flahaut, Bahcine Bakiz, Pawel Nowakowski, Jean-Raymond Gavarri

Electrical properties and reactivity under air–CO flows of composite systems based on ceria coated carbon nanotubes

M. David [a], M. Arab [a,*], F. Guinneton [a], E. Flahaut [b], B. Bakiz [a], P. Nowakowski [a], J.R. Gavarri [a]

[a] *Université du Sud Toulon – Var, IM2NP, UMR CNRS 6242, BP 20132, F 83 957 La Garde, France*
[b] *Universite Paul – Sabatier, CIRIMAT, UMR CNRS 5085/LCMI, F 31062 Toulouse cedex 4, France*

Keywords:
Carbon nanotubes
Cerium dioxide
Microstructural analyses
Electrical conduction
Infrared spectroscopy
Solid–gas interactions

A B S T R A C T

Nanocomposite systems of ceria nanoparticles and Double Walled Carbon Nanotubes (DWNTs) coated with nano-ceria (n-CeO_2) were elaborated using a classical sol gel method. Three samples noted as [n-CeO_2 + xDWNTs] with variable weight fractions x = 0, 5 and 15 wt.% of DWNTs were obtained. The samples were characterized by X-ray diffraction and electron microscopy. The electrical conductivity of [n-CeO_2 + xDWNTs] compacted pellets systems was determined from electrical impedance spectrometry, under air, between 120 and 400 °C. In this temperature range, all samples were semi-conducting with a weak variation of activation energy. However, the conductivity strongly increased with the weight fraction of ceria coated carbon nanotubes. Finally, the solid–gas interactions between air–CO flows and these systems were studied as a function of time and temperature, by means of Fourier transform infrared (FTIR) spectroscopy. The oxidation kinetics of CO into CO_2 was analyzed from the evolutions of FTIR absorption band intensities. As the carbon nanotube fraction x increased, the conversion efficiency was strongly improved.

1. Introduction

Nanocomposites made on carbon nanotubes present many advantages like hollow nanotubular structure and new properties. Nanocomposites based on carbon nanotubes (CNTs) offer a promising application in electrochemistry, catalysis, electronic conduction, gas storage, etc. They are also suitable materials as electrodes in double layer capacitors [1,2].

Studies on CeO_2 (ceria) nanoparticle assemblies were extensively developed in the past as electrolyte materials in solid-state oxide fuel cell. Ceria was investigated as ionic conductor, electronic promoter of heterogeneous catalytic reactions, oxygen storage capacitor in industrial catalytic processes such as automotive exhaust emission control [3–5].

In recent years, several studies were conducted on one-dimensional nanostructures such as nanorods [6,7], nanowires [8] and nanotubes [9,10]. CNTs based materials have attracted many technological and scientific interests: due to their remarkable properties linked to their tubular form and their nanoscale [11,12], they could offer exciting possibilities for a lot of applications including miniaturized and faster electronic devices. Carbon nanotubes seem also to be ideal for adsorption [13–16], sieving [17] and gas detection [18–21], due to their high specific surface and porosity. Chemical functionalization of carbon nanotubes would allow enhancing their electrical conductivity and generating new properties.

In this work, the double wall carbon nanotubes (DWNTs) were chosen because they exhibit an intermediate form between the single wall carbon nanotubes (SWNTs) and the multi walled ones. The DWNTs combine numerous advantages: they present morphologies and properties similar to those of the SWNTs, and the outer carbon nanotube can provide an efficient protection of the inner one. In this case, the structure and properties of the inner tube would remain unchanged [22].

Recently [23–26], a study of the catalytic properties of composite systems based on ceria and carbon nanotubes coated by ceria has shown that these systems could be interesting to convert carbon monoxide into CO_2. The originality of this work is to keep the composite ceria and DWNTs in its configuration as long as one-dimensional structure, with carbon nanotubes as template during the study. Nanocomposites without the carbon skeleton may lose their tubular structure (diameter reduction, therefore surface area) as a function of temperature [25]. Unlike ceria tubes only have a high electrical resistance; we exploit the conductive character of the carbon nanotubes to modify the electrical and catalytic properties.To our knowledge, this is the first time that catalytic studies are conducted on these composites with carbon nanotubes and trying to link the transfer of charge conduction in the CO conversion mechanism.

* Corresponding author. Tel.: +33 494142533; fax: +33 494142168.
E-mail address: madjid.arab@univ-tln.fr (M. Arab).

doi:10.1016/j.cej.2011.03.079

The general aim of this study was to develop new anisotropic materials having absorbing and/or filtrating properties for gas selectivity in sensor applications. In this work, we first elaborate nanocomposite systems [n-CeO_2 + xDWNTs] in which x is the weight fraction of double wall carbon nanotubes and n-CeO_2 is nano-ceria. Then, we determine the electrical conduction properties of compacted samples constituted of these nanocomposite systems, in the temperature range of 100–400 °C: in this temperature range, the stability of carbon nanotubes (coated with ceria) is ensured. Then, we characterize the solid–gas interactions between air–CO flows and these nanocomposite systems. The experimental approach consists in determining the conversion of CO into CO_2 as a function of time and temperature, making use of Fourier transform infrared (FTIR) spectroscopy. The samples are characterized using X-ray diffraction (XRD) and scanning and transmission electron microscopies (SEM, TEM).

2. Experimental

2.1. Synthesis

The nanocomposite system has been synthesized following two different steps: carbon nanotubes synthesis and ceria coating of nanotubes. This approach based on precipitation way is reported in previous works by several authors using carbon nanotubes (multi wall) [17–20] and anodic alumina membrane (AAM) [27] as template method. In our work, DWNTs are used as support for ceria nanoparticles.

As a first step, the DWNTs were produced by catalytic chemical vapour deposition (CCVD) from a H_2–CH_4 gas mixture using an oxide (Mg, Co, Mo)O catalyst. Details of the synthesis were previously reported by Flahaut et al. [28,29]. Then, as a second step, a composite synthesis was performed. The carbon nanotubes (variable amounts of DWNTs) were first refluxed in a 30% nitric acid solution at 140 °C for 24 h. The as treated DWNTs were dispersed in 50 mg/ml $Ce(NO_3)_3$ solutions, in ultrasonic bath at room temperature, for 1 h. Under heavy stirring, the pH of solutions were controlled and adjusted close to pH 9, by slowly adding NaOH solution. After rinsing with deionised water and drying at 80 °C, the final composite samples were obtained. The as-prepared final samples were maintained under air at high temperature for calcinations with a heating rate of 5 °C/min from room temperature to 450 °C for 1 h. After calcination setup, the color of the composite materials (noted as [n-CeO_2 + xDWNTs] where x is the weight fraction) changes from yellow for ceria nanoparticles, to dark gray for the composite system.

Three types of composite samples were prepared: (i) a CeO_2 nanopowder (noted n-CeO_2, (ii) a 5 wt.% composite [n-CeO_2 + 5 wt.% DWNTs], and (iii) a 15 wt.% composite [n-CeO_2 + 15 wt.% DWNTs]. It should be noted that the volume fractions of DWNTs coated by ceria are obviously larger than their weight fractions, because of the very low density of DWNTs [30]. In addition, the apparent specific surfaces areas of assemblies of nanotubes (external current dimensions 500 nm × 20 nm) are strongly weaker than the specific surface areas of ceria isolated grains (isotropic dimension of 10 nm).

2.2. Materials characterizations

2.2.1. X-ray diffraction (XRD)

Each sample was first characterized by XRD to identify the phases and to determine the mean size of particles. X-ray diffraction patterns were recorded on a Siemens-Brucker D5000 diffractometer working in a θ–2θ mode, with a copper X-ray source ($\lambda(K\alpha_1)$ = 1.5406 Å), Soller slides, and secondary monochromator.

2.2.2. Microstructural techniques

Scanning and transmission electron microscopy analyses were used to observe the nanoparticles morphology. Preliminary images were obtained with a Philips XL30 SEM using a maximum voltage of 20 kV. TEM analyses were carried out using a Tecnai G^2 microscope with a LaB_6 source, operating at 200 kV.

2.2.3. Electrical impedance spectrometry

The various polycrystalline samples were compacted under a pressure of 3 kbar in the form of cylindrical pellets and subjected to impedance spectroscopy analyses. The equipment was a SOLARTRON impedancemeter, the frequency varying between 1 and 10^7 Hz. The cylindrical pellets were placed between platinum electrodes, in a specific heating cell, and the cell was introduced in a furnace, under air. All measurements occurred in the temperature range of 100 °C–450 °C.

2.2.4. Catalytic analysis

The catalytic conversion of CO gas in air–CO mixtures was analyzed using FTIR spectroscopy adapted to gas analysis. The apparatus was a Mattson–Bruker equipment (cube corner technique). The composite samples were exposed to air–CO gas flows in a specific homemade heated cell. This homemade device was previously described in ref. [31]. The samples were fixed between two inert separators and placed in isothermal area into the reactor which is connected to a gas platform with CO and synthetic air. The constant masses of samples (100 mg) were degassed at 450 °C before measurements. The gas flow (2500 ppm CO in air with a fixed speed at 10 ml/min) is injected in the quartz cell containing the separators and the sample. Then, the gases transformed or not by the catalytic action of the sample, were directed to a cylindrical FTIR analyzer cell to be subjected to FTIR analysis.

The spectra FTIR acquisitions were carried out every 30 s, during 1 h, after background analysis under neutral atmosphere. After FTIR measurements, the appearance of the new absorption band was observed, corresponding to the CO_2. The results give rise to the overall reaction:

$$CO + 1/2\,O_2 \rightarrow CO_2 \quad (1)$$

The conversion kinetics is directly determined using the CO_2 absorption band intensities (in arbitrary units) as a function of time and temperature. The catalytic conversion rate of CO into CO_2 was defined as being proportional to the intensity of the FTIR CO_2 vibrational band (doublet at 2340–2360 cm^{-1}). We noted $I(CO_2)$ as the intensity corresponding to the area under CO_2 picks band absorption.

All tests were reproduced several times (an average 10 times) with different samples to ensure result reproducibility.

3. Results

3.1. Microstructures

Fig. 1 shows the TEM images of CeO_2 and carbon nanotubes. Fig. 1a shows long threads of DWNTs before composite preparation process: they form bundles having thicknesses ranging between 3 (single CNT) and 30 nm.

In the case of the x = 5 and 15 wt.% samples, we obtained ceria coated nanotubes having lengths ranging between 200 and 500 nm and thicknesses ranging between 40 and 60 nm. The initial DWNTs seem to be continuously covered with CeO_2 nanoparticles having mean sizes of 10 nm. The ceria coating has a granular (porous) polycrystalline aspect with a thickness of about 20 nm (see Fig. 1b). The initial channel structures of the DWNTs are observable as being clear tubular zones inside the ceria nano-tubular structures.

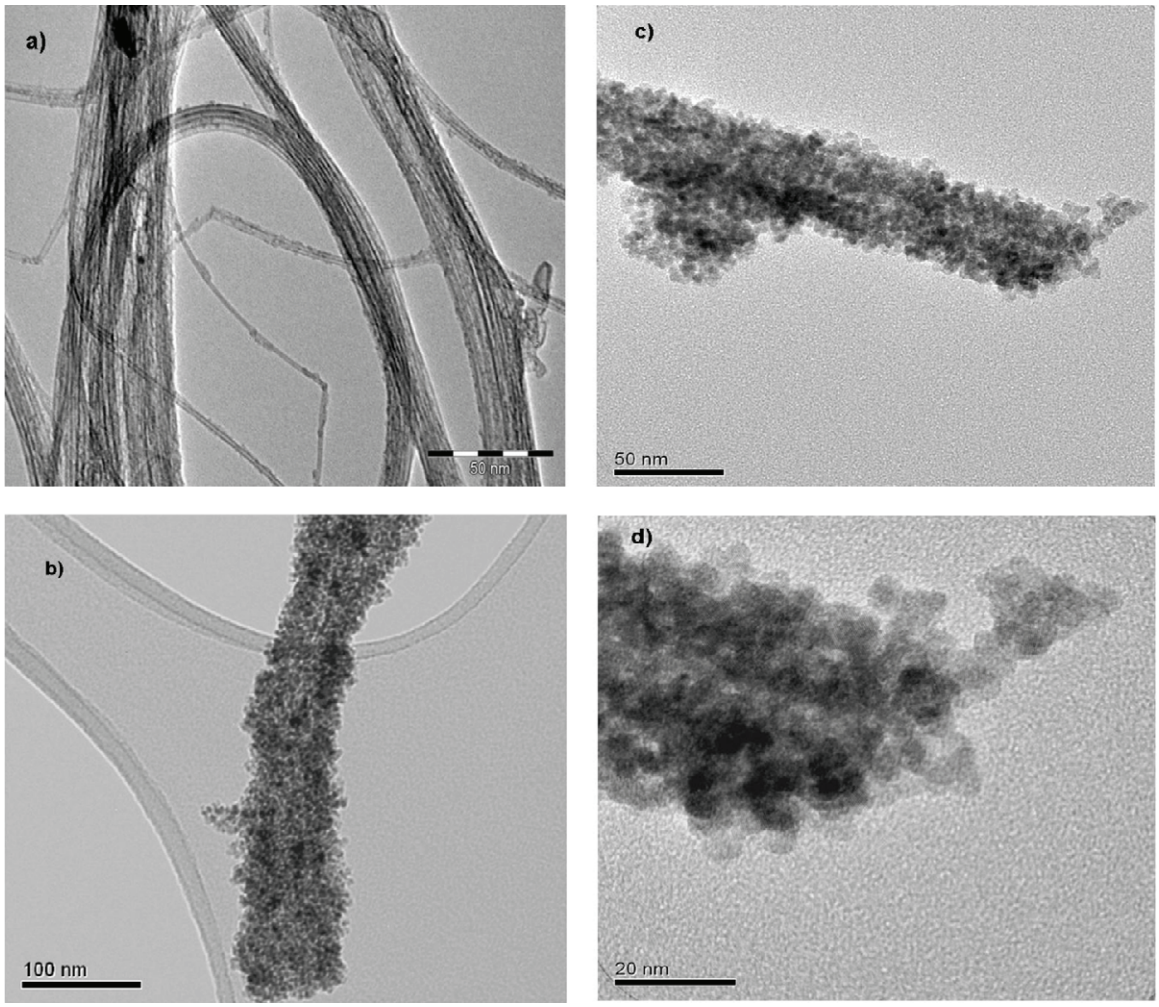

Fig. 1. TEM images (5 wt.% sample). (a) Threads of initial DWNTs (before composite synthesis), bundle of nanotubes coated by ceria nanograins with its internal light grey zone: (b) and (c) for the $x = 5$ and 15 wt.% respectively; (d) detail of ending part of 15 wt.% sample.

It should be noted that the inner diameter corresponds to the diameters of isolated DWNTs bundles.

Fig. 2 represents the typical X-ray diffraction patterns obtained from the pure nanocrystalline ceria sample, and for the $x = 15$ wt.% composite sample. In full agreement with literature results [17–19,32], the two characteristic Bragg peaks of CNTs corresponding to the (0 0 2) and the (1 0 1) in the XRD pattern, are observed in this last sample close to the angle of $2\theta = 26.5^{\circ}$. The ceria polycrystalline phase is clearly evidenced through the Bragg peaks of fluorite structure (JCPDS 89-8436): these diffraction peaks are systematically broadened, which confirms the nanostructuration of ceria phase. The mean grain size has been calculated using the Scherrer formula: $D = 0.9\,\lambda/\Delta(2\theta)\cos\theta$

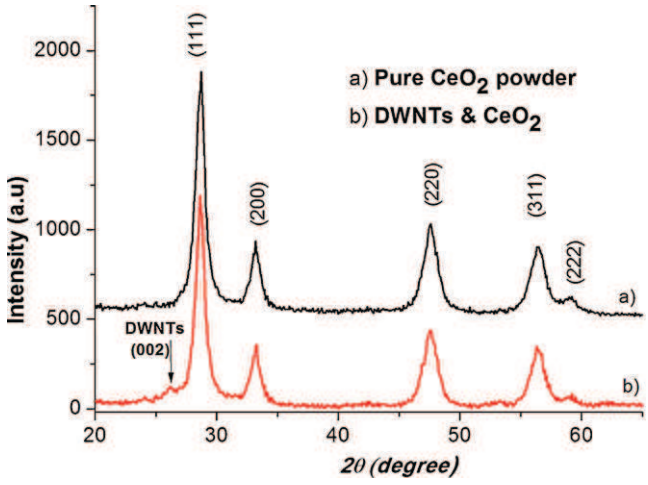

Fig. 2. (a) X-ray diffraction pattern of nano-ceria and; (b) 15% ceria coated carbon nanotubes with presence of classical DWNT (0 0 2) – (1 0 1) diffraction peaks. Bragg peak broadening is related to size effect in ceria fluorite lattice.

In this expression, λ is the wavelength, θ is the classical Bragg angle, $\Delta(2\theta)$ is the Bragg peak broadening determined from $\Delta(2\theta) = [(\Delta(2\theta)_{exp}) - (\Delta(2\theta)_{stand})]$ where $\Delta(2\theta)_{exp}$ and $\Delta(2\theta)_{stand}$ are respectively the observed and standard full widths at half maximum (FWHM). The $\Delta(2\theta)$ difference is the broadening resulting from size effect, calculated in the Lorentzian profile approximation. Using this Scherrer model, we have determined mean sizes of 12 nm for ceria grains in each sample.

3.2. Electrical properties under air

Electrical measurements are performed with different samples: DWNTs, ceria oxide respectively alone and the composites [n-CeO_2 + xDWNTs].

The Nyquist representations (Fig. 3a–c) for experiments performed between 100 and 400 °C were characterized by one or two circles in the Nyquist plane ($Z = Z' + jZ''$; $X = Z'$, $Y = -Z''$). The circle

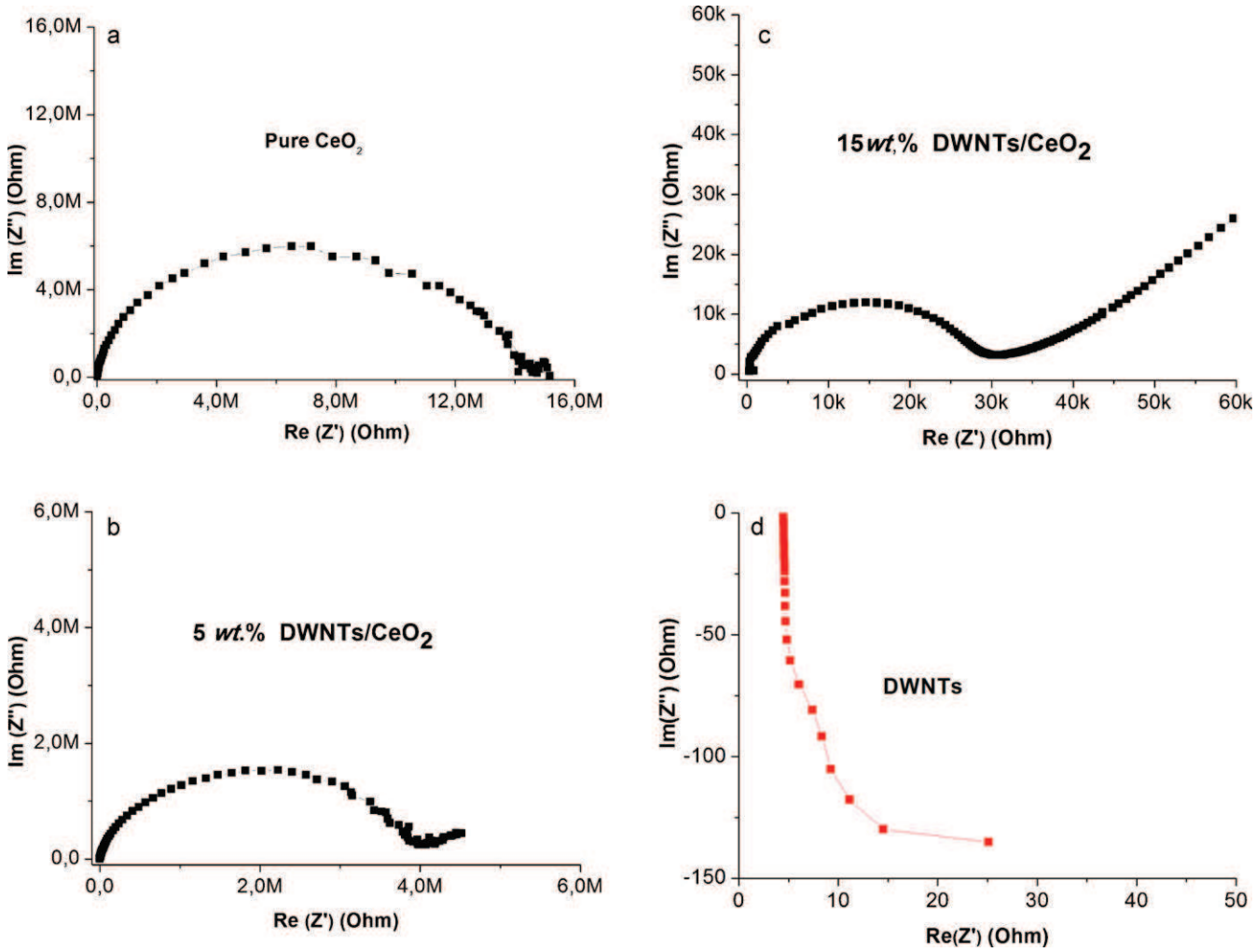

Fig. 3. Typical Nyquist representations obtained at 360 °C of the samples: (a) ceria powder, (b) and (c) [n-CeO_2 + *x* DWNTs] with *x* = 5 and 15 wt.%, (d) DWNTs powder.

associated with high frequencies was attributed to grain cores and ceria coated nanotubes. The circle associated with low frequencies was attributed to grain boundaries and electrode interfaces. However, the response of alone DWNTs (Fig. 3d) shows a very high conductance with an induction effect due to the metallic character of the nanotubes [33] (*equivalent to a short circuit*). In addition, the measured resistance value is not reliable because the generated resistive barriers of the electrodes and measurement apparatus are in the same order of magnitude.

To analyse these Nyquist plots, we have used classical electrical circuits based on the following expression for the impedance *Z*:

$$\frac{1}{Z} = \frac{1}{R} + (jC^*\omega)^n$$

In this expression, *R* is the resistance (in Ω), C^* is a constant and *n* is an exponent characteristic of the material heterogeneity: C^* is a capacity expressed in farad unit only for $n = 1$.

The resistances of grain cores R_{core} were determined from the intersection of the high frequency circle with the horizontal axis of Nyquist diagram. Depletion angles $\delta = (1 - n)\pi/2$ of these Nyquist circles have been determined. They generally result from heterogeneities and porosity in samples.In the table below, as the carbon nanotube fraction *x* increases, we observe a strong decrease in resistance *R*, a relatively weak increase in C^* and a significant decrease in exponent *n*. This last feature is clearly due to the specific microstructure of the composites systems: as the carbon nanotube fraction increases, the systems present an increasing degree of heterogeneity associated with the large differences (i) in grain dimensions (nanosized ceria grains and larger coated nanotubes) and (ii) in electrical conduction behaviours (ceria is semi-conducting, carbon nanotubes have a metallic character). At low frequency, we observe a typical Warburg-like behaviour corresponding to diffusion at the electrodes.

The apparent conductivity (noted σ) of each compacted material has been calculated from these resistance values (*R*) using the classical relation:

$$\sigma = \frac{1}{R} \cdot \frac{L}{S}$$

where *R*, *L* and *S* are successively the resistance, the thickness and the electrode surface.

In Fig. 4a, we have reported the variation of the logarithm of conductivity log ($\sigma(x,T)$) with the weight fraction *x* of nanotubes and at various temperatures *T* (120, 160, 200, 240, 300, 350, 400, 440 °C). In Fig. 3b, we have represented the evolution of the logarithm of conductivity, log ($\sigma(x,T)$) as a function of $1/T$ (Arrhenius plots with *T* in Kelvin).

From these data, we observe that the three samples (0, 5 and 15 wt.%) present a global semiconducting behaviour with activation energies E_{act} close to 1 eV.

The main result resides in the strong increase in conductivity with the fraction of nanotubes: the conductivity of the 15% sample is 1000 times higher than the one of ceria sample for a fixed temperature. This means that ceria coated carbon nanotubes could

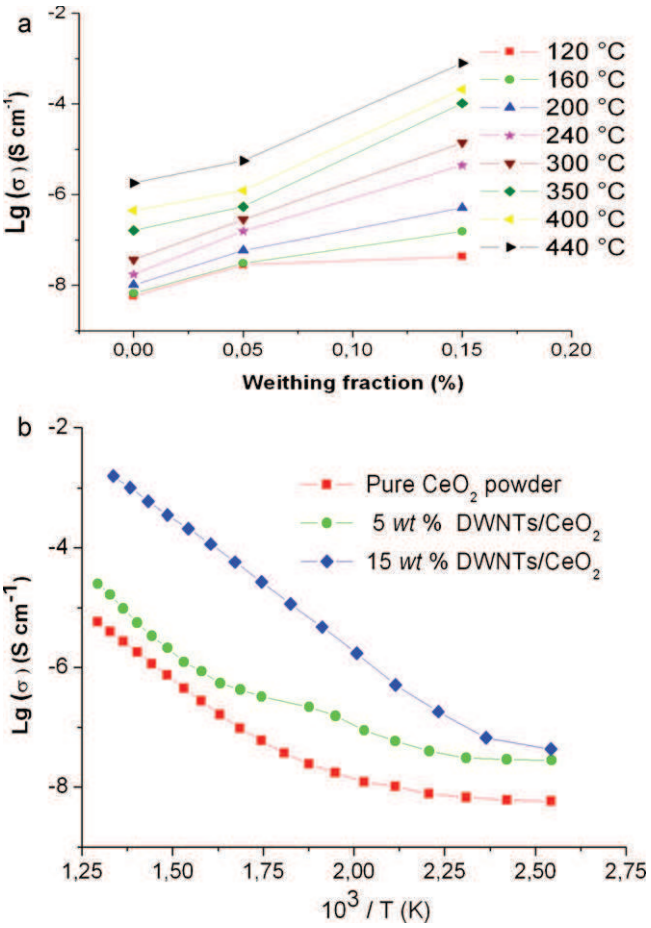

Fig. 4. (a) Variation of conductivity with the weight fraction x of DWNTs at various temperatures: logarithmic increase in conductivity due to DWNTs. (b) Variation of conductivity with temperature in Arrhenius representation for the three samples: nano-ceria powder and n-CeO_2 + xDWNTs with x = 5 and 15 wt.%.

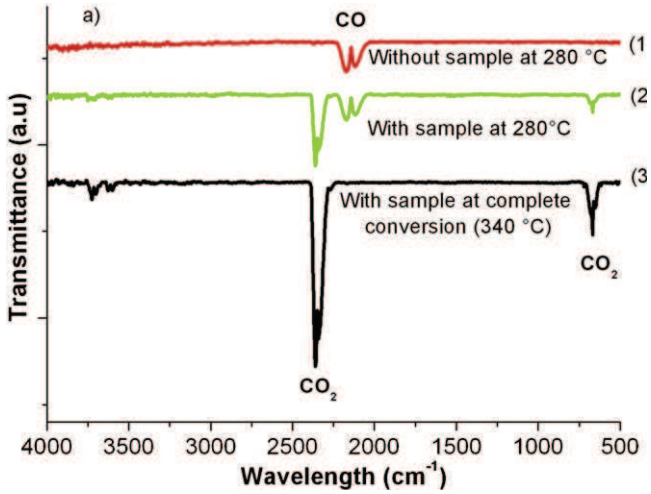

Fig. 5. FTIR vibrational bands for CeO_2/5 wt.% DWNTs sample: (1) without sample; (2) partial conversion with sample; (3) complete conversion with sample.

be characterized by an increasing population of charge carriers due to the internal carbon nanotubes, and increasing electron mobility due to these nanotubes. However, as all DWNTs agglomerates are enveloped in nano-ceria coating, a barrier due to this envelop should condition the observed semi-conducting character. In the case of this composite medium, the resulting behaviour will be a compromise between the two semi-conducting behaviours of pure ceria and ceria coated nanotubes.

3.3. Solid–gas interactions and FTIR analyses

Fig. 5 shows the infrared spectra of CO and CO_2 absorption bands observed at 280 °C and 340 °C obtained respectively with and without sample (5 wt.%). In presence of active samples, the spectra are characterized by the appearance of a new absorption band corresponding to the emission of CO_2 resulting from CO conversion. As temperature increases, a complete conversion occurs (360 °C for ceria powder and 340 °C for composites).

Fig. 6a–c represent the time dependent evolutions of the CO_2 FTIR band intensity at various temperatures, for the three samples. The decrease in CO band intensities is clearly correlated with the increase in CO_2 band intensities. At 340 °C, the conversion reaches a maximum level (the CO band vanishes and the CO_2 band reaches a constant value).

The solid–gas interactions are based on three main physicochemical steps: gas adsorption process, surface reactions and then gas desorption process. Two different mechanisms have been proposed to describe these reactions: the Langmuir–Hinshelwood mechanism [34], and the Mars–Van Krevelen mechanism [35]. The first mechanism is relative to reactions between adsorbed CO gases and adsorbed oxygen (O_2) from air. The second mechanism is relative to the recombination of adsorbed CO gas with the oxygen present at the oxidized surface sites. This last mechanism is stimulated by diffusion process of oxygen vacancies.So, for CO and carbon nanotubes interaction, no catalytic mechanism as described previously is applicable because the DWNTs are stable in the studied temperature range. The CO adsorption/desorption on carbon nanotubes follow the physisorption process with low charges transfer as reported in previous work [16].

Fig. 6a–c show that the mechanism of conversion starts from 180 °C and reaches a maximum of efficiency at a temperature close to 340 °C. For a fixed temperature, the conversion increases, and then reaches a constant value after an initiating period of about 20 min.

Fig. 7 represents the maximum values reached by the CO_2 band intensities as a function of temperature. These data clearly show that the $I(CO_2)$ conversion intensity strongly increases with DWNTs fraction: a factor of 2.5 is obtained between the intensities of the 15 wt.% sample and pure ceria powder (without DWNT) at 300 °C. This increase in conversion intensity with DWNTs fractions cannot be attributed to any increase in specific surface of samples: as x increases, the proportion of large composite n-CeO_2–carbon nanotubes, having smaller specific surfaces, increases. It is necessary to remind that the ceria coated carbon nanotubes have an average dimension (500 nm × 50 nm) larger than the dimensions of isolated ceria nano-grains (linear dimension of about 10 nm). If the nature of solid–gas interactions was assumed unchanged in all samples, then we could have expected a decreasing reactivity of the composite samples, because of decreasing number of active sites (the catalytic efficiency, therefore active sites number, was mainly correlated to the grain size) [36]: this is not the case in our experiments. So, we can conclude that ceria coated carbon nanotubes present specific catalytic activities and are at the origin of the improved conversion of CO into CO_2. Fig. 8 shows that, as DWNT fraction increases, the catalytic action starts at a lower temperature, and that a strong improved conversion rate is observed at intermediate temperatures (from 250 to 340 °C). At 340 °C, the conversion of CO is maximum for the two composites 5 and 15 wt.%. We also observed at the same temperature, the catalytic efficiency (Fig. 7) is higher for the 15 wt.% sample.

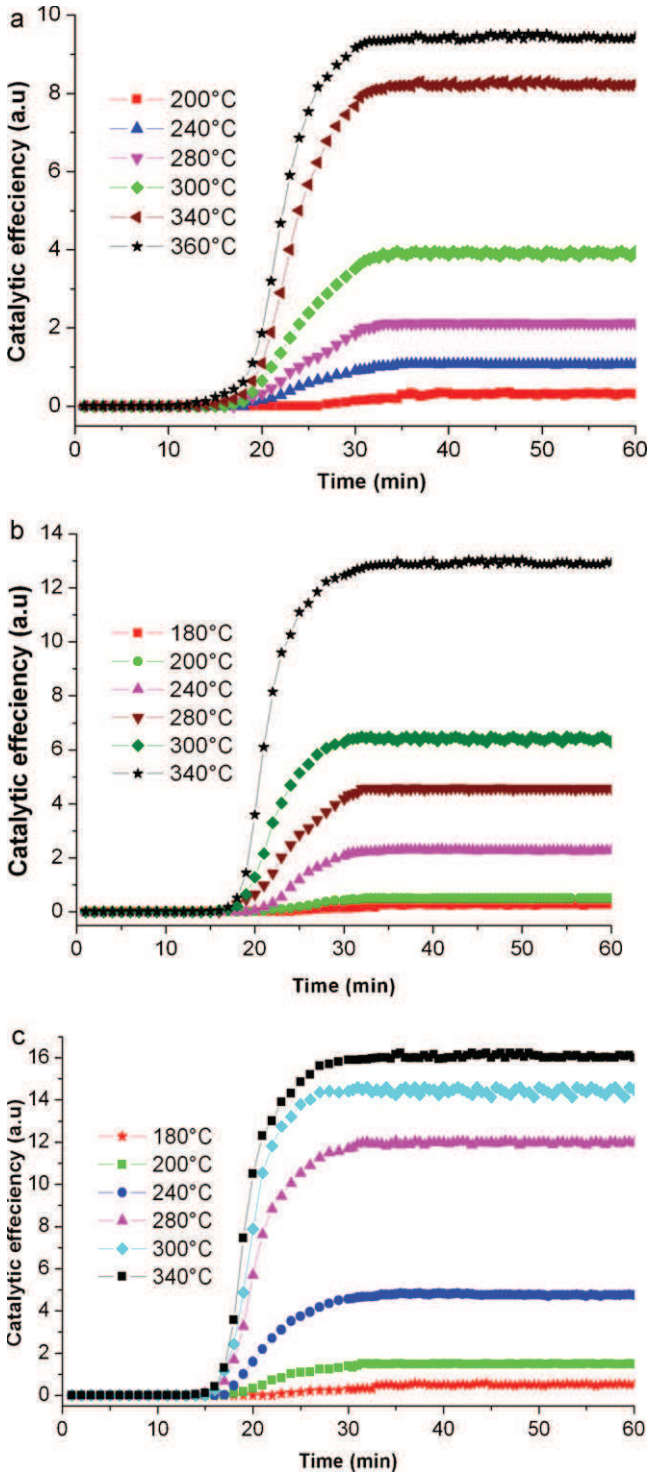

Fig. 6. Variations of intensities of CO_2 absorption bands versus time, at different temperatures (a) for pure nanostructured ceria sample; (b) for sample $x = 5$ wt.%; (c) for sample $x = 15$ wt.%.

Our results can be compared with previous results obtained by gas chromatography (GC) [17–20]: the authors showed that the catalytic activity started from 50 °C (which corresponds to the beginning of the CO conversion). They observed that the complete CO conversion systematically occurred at 300 °C for all samples: in their work, the authors investigated nano-ceria, nanorods and individual nanotubes (without any DWNTs support). In our case, there is a shift of 40–50 °C with a starting reactivity close to 100 °C and

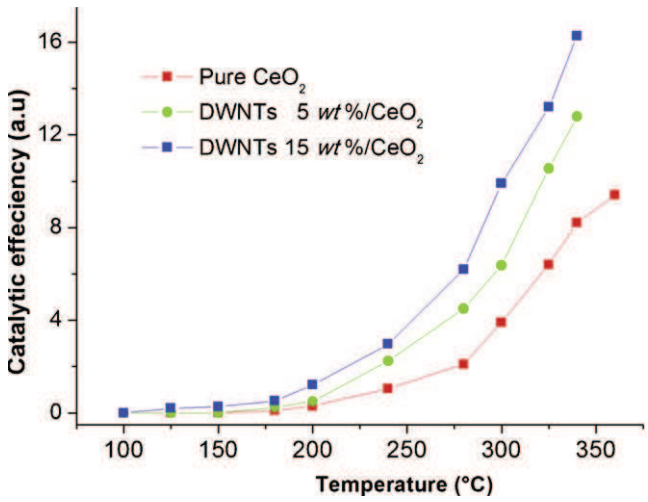

Fig. 7. Catalytic efficiencies as a function of temperature for the three samples.

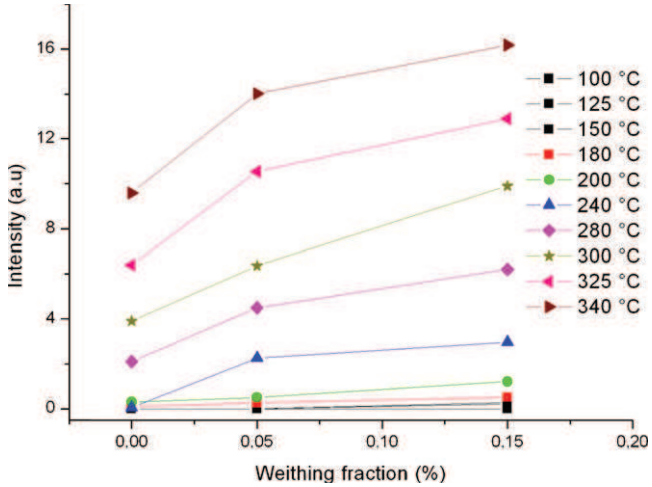

Fig. 8. Variation of CO_2 band intensities versus composition x, at various temperatures. Strong increase in catalytic efficiency as DWNT content x increases.

a complete conversion at 340 °C. This difference is due first to the nature of our samples (composite CeO_2/DWNTs), and secondly, to the analysis method (GC vs FTIR).

In both cases, the as prepared composites (CeO_2/DWNTs) had better CO catalytic activity than ceria nanoparticles. This means that morphology and electrical nature could condition the catalytic performance of these materials, which is in agreement with the results reported by the authors [17–20].

4. Discussion

In this study, two different results have been obtained: as the DWNTs fraction increased, the conductivity of compacted composites increased (however with a semiconducting behaviour) and the catalytic conversion of CO into CO_2 was improved. A tentative approach to correlate these two results might be proposed. The semiconducting behaviour of the three studied samples is probably due to the specific microstructure of the conducting (metallic) carbon nanotubes coated or encapsulated in a thick coating of ceria. The internal carbon skeleton could deliver highly mobile electrons; the ceria layer constituted of ceria nano-grains could play the role of a porous barrier, with charges migrating along grain boundaries or tunnelling through this partial insulator. The conduction is mainly due to the charge carrier displacement in the oxide grains,

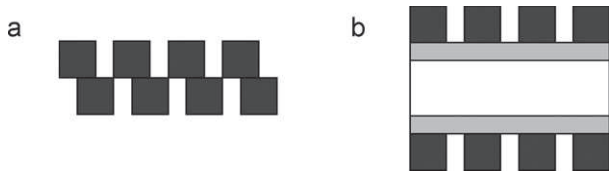

Scheme 1. Model of space occupation of idealized 8 cubic grains: (a) agglomerates of 8 isolated nano-ceria grains; (b) nano-ceria grains enveloping a nanotube. Given the higher dimensions of nanotubes, the ratio S/V is lower in the case of ceria particles covering nanotubes.

on the carbon nanotubes surfaces and at the ceria carbon nanotubes interfaces. So, the conduction occurs through the barriers at the generated interfaces. This specific microstructure could also be at the origin of the improved catalytic properties observed in our study. First, it should be reminded that the specific surface areas of ceria coated nanotubes decrease as the DWNTs fraction increases. This is due to the fact that the ratio S/V of the total surface S of ceria grains over the total volume V of these ceria grains is weaker for isolated ceria grains than for ceria grains enveloping carbon nanotubes. This is modeled by Scheme 1. Consequently, the catalytic improvement has to be attributed to the increasing contribution of carbon nanotubes and their interfaces with ceria. More precisely, the increased capacity to exchange electrons with external molecules (CO and O_2) of the ceria porous layer associated with carbon nanotubes could be at the origin of this improved conversion of CO into CO_2.

The reaction at the surface of the ceria solid should be:

$$CO \rightarrow CO\,(\text{adsorbed on solid})$$

$$O_2\,(\text{adsorbed on solid}) \rightarrow 2\,O\,(\text{adsorbed on solid})$$

$$O^{2-}\,(\text{from ceria lattice}) \rightarrow O^{*}\,(\text{on ceria surface}) + 2\,e^{-}\,(\text{in ceria lattice})$$

or

$$O^{-}\,(\text{from ceria lattice}) \rightarrow O*\,(\text{on ceria surface}) + e^{-}\,(\text{in ceria lattice})$$

When an oxide material is exposed to air, O_2 molecules can be adsorbed on the surface, and could be ionized into O^{2-} or O^{-} ions by capturing free electrons from the [n-CeO_2 + xDWNTs] composite.

In absence of DWNTs, the electrons could be mainly located on Ce^{3+} cations present in nonstoichiometric nano-ceria:

$$2Ce^{4+} + 2e^{-} \rightarrow 2\,Ce^{3+}$$

In presence of DWNTs, the electrons of ceria could be quickly exchanged with these DWNTs (because of contacts ceria/DWNT). In such circumstances, all local electronic processes could be accelerated, thus improving the conversion of CO into CO_2. This can be described as follows:

$$CO + O^{2-} \rightarrow CO_2 + 2\,e^{-}$$

and

$$CO + O^{-} \rightarrow CO_2 + 1e^{-}$$

This mechanism is stimulated by diffusion process of oxygen vacancies at high temperature.

5. Conclusion

In this work, a nanocomposites n-CeO_2 + xDWNTs were obtained using a simple route based of precipitation of ceria nanoparticles on functionalized DWNTs. The obtained samples depending on the amount of carbon nanotubes show good electrical and catalytic properties. We observed that the catalytic activity increases as carbon nanotubes quantity increases in the temperature range of 100 C–360 °C. The complete conversion of CO into CO_2 occurred at 340 °C, with a greater efficiency for the sample to 15 wt.% of DWNTs compared to the ceria powder.

The conductor nature of the carbon nanotubes allowed the composites to became more semiconductor, which the electrical conductivity increase as function of DWNTs. carbon nanotubes promote charges carriers transfer.

These results show that the presence of DWNTs plays a determining role in the catalytic mechanism and the conversion efficiency of CO.

These systems could be used as sensitive materials for CO detection, and are being integrated on gas sensor devices.

References

[1] T.S. Ahmadi, Z.L. Wang, T.C. Green, A. Henglein, M.A. Sayed, Science 272 (1996) 1924.
[2] G. Che, B.B. Lakshmi, E.R. Fisher, C.R. Martin, Nature 393 (1998) 346.
[3] J. Zhang, X. Ju, Z.Y. Wu, T. Liu, T.D. Hu, Y.N. Xi, Chem. Mater. 13 (2001) 4192.
[4] G. Balducci, M.S. Islam, J. Kaspar, P. Fornasiero, M. Graziani, Chem. Mater. 12 (2000) 677.
[5] T. Sayle, C. Parkerb, D.C. Sayle, Chem. Commun. (2004) 13563.
[6] A. Vantomme, Z.-Y. Yang, G. Du, B.-L. Su, Langmuir 21 (2005) 1132–1135.
[7] P.X. Huang, F. Wu, B.-L. Zhu, X.P. Gao, H.Y. Zhu, T.Y. Yan, W.P. Huang, S.H. Wu, D.Y. Song, J. Phys. Chem. B 109 (2005) 19169–19174.
[8] S. Chunwen, L. Hong, W. Zhaoxiang, C. Liquan, H. Xuejie, Chem. Lett. 33 (2004) 662–668.
[9] W.-Q. Han, L. Wu, Y. Zhu, JACS 127 (2005) 12814–12815.
[10] K. Zhou, Z. Yang, S. Yang, Chem. Mater. 19 (2007) 1215–1217.
[11] R.H. Baughman, A.A. Zakhidov, W.A. De Heer, Science 297 (2002) 787.
[12] X.G. Peng, L. Manna, W. Yang, J. Wickham, Nature 404 (2000) 59.
[13] M. Bienfait, et al., Physica. B 350 (2004) 423.
[14] M.R. Babaa, I. Stepanek, K. Masenelli-Varlot, N. Dupont-Pavlovsky, E. McRae, P. Bernier, Surf. Sci. 531 (2003) 86.
[15] H. Ulbricht, G. Moos, T. Hertel, Surf. Sci. 852 (2003) 532.
[16] M. Arab, F. Picaud, M. Devel, C. Ramseyer, C. Girardet, Phys. Rev. B 69 (2004) 165401.
[17] M. Arab, F. Picaud, C. Ramseyer, M.R. Babaa, F. Valsaque, E. McRae., J. Chem. Phys. 126 (2007) 054709.
[18] R. Langlet, M. Arab, F. Picaud, M. Devel, C. Girardet, J. Chem. Phys. 121 (2004) 9655.
[19] S. Chopra, K. McGuire, N. Gothard, A.M. Rao, A. Pham, Appl. Phys. Lett. 83 (2003) 2280.
[20] C. Cantalini, L. Valentini, I. Armento, L. Lozzi, J.M. Kenney, S. Santucci, Sens. Actuator, B 95 (2003) 195.
[21] M. Arab, F. Berger, F. Picaud, C. Ramseyer, J. Glory, M. Mayne-L'Hermite, Chem. Phys. Lett. 433 (2006) 175.
[22] Y.F. Li, R. Hatakeyama, T. Kaneko, T. Izumida, T. Okada, T. Kato, Nanotechnology 17 (2006) 4143.
[23] J. Fang, Z. Cao, D. Zhang, X. Shen, W. Ding, L. Shi, J. Rare Earths 26 (2) (2008) 153.
[24] Z.-C. Di, J. Ding, X.-J. Peng, Y.-H. Li, Z.-K. Luan, J. Liang, Chemosphere 62 (2006) 861–865.
[25] D. Zhang, H. Fu, L. Shi, J. Fang, Q. Li, J. Solid State Chem. 180 (2007) 654–660.
[26] D. Zhang, C. Pan, L. Shi, L. Huang, J. Fang, H. Fu, Microporous Mesoporous Mater. 117 (2009) 193–200.
[27] R.-J. La, Z.-A. Hu, H.-L. Li, X-Li. Shang, Y.-Y. Yang, Mater. Sci. Eng. A368 (2004) 145–148.
[28] E. Flahaut, R. Bacsa, A. Peigney, C. Laurent, Chem. Commun. (2003) 1442–1443.
[29] E. Flahaut, Ch. Laurent, A. Peigney, Carbon 43 (2005) 375.
[30] Ch. Laurent, E. Flahaut, A. Peigney, Carbon 48 (2010) 2989–2999.
[31] P. Nowakowski, S. Villain, A. Kopia, I. Suliga, J.R Gavarri, Appl. Surf. Sci. 254 (2008) 5675.
[32] X. Peng, Z. Luan, J. Ding, Z. Di, Y. Li, B. Tian, Mater. Lett. 59 (2005) 399–403.
[33] V. Zólyomi, Á. Rusznyák, J. Kürti, Á. Gali, F. Simon, H. Kuzmany, Á. Szabados, P.R. Surján, Phys. Status Solidi B 243 (13) (2006) 3476–3479.
[34] H. Over, M. Muhler, Prog. Surf. Sci. 72 (2003) 3.
[35] G. Martinelli, M.C. Carotta, Sens. Actuators, B 23 (1995) 157.
[36] P. Nowakowski, J.-P. Dallas, S. Villain, A. Kopia, J.-R. Gavarri, J. Solid. State Chem. 181 (2008) 1005–1016.